Supplementary Information

Microfluidic device-fabricated spiky nano-burflower shape gold nanomaterials facilitate large biomolecules delivery into cells using infrared light pulses

*Kavitha Illath [a], Srabani Kar [b], Ashwini Shinde [a], Rajdeep Ojha [c], Dhanya R Iyer [d], Nitish R Mahapatra [d], Moeto Nagai [e] and Tuhin Subhra Santra [a]**

[a] Department of Engineering Design, Indian Institute of Technology Madras, India

[b] Department of Electrical Engineering, University of Cambridge, UK

[c] Department of Bioengineering, Christian Medical College, Vellore, India

[d] Department of Biotechnology, Indian Institute of Technology Madras, India

[e] Department of Mechanical Engineering, Toyohashi University of Technology, Aichi, Japan

Corresponding author: *santra.tuhin@gmail.com & tuhin@iitm.ac.in

Table S1. Overview of notable works on microfluidic-based intracellular delivery platform.

Microfluidic platform	Biomolecule	Cell line	Cell viability	Delivery efficiency/ fluorescence intensity (a.u.)	Ref.
Cell squeezing	Dextran 3 kDa	HeLa	~ 90 %	< 80 %	1
	Carbon nanotubes	HeLa	~ 95 %	~ 60 %	
	siRNA	HeLa	-	~ 90 % (gene knockdown)	
	anti-tubulin antibodies	HeLa	~ 75 %	~ 95 %	
	Dextran 40 kDa	K562 3.21 Jurkat	83 % 94 %	57 % 65 %	2
	EGFP	Jurkat	73 %	45 % (protein expression)	
Vertical edge	4-2000 kDa, Plasmids & 100 nm particles	K562	< 5 % (cell death)	~ 90 %	3
Flow-through electroporation	GFP	CT26 K562	< 60 % ~ 75 %	~ 65 % ~ 62 %	4
Microfluidic electroporation	Plasmid DNA	HeLa	~ 97 %	~ 99 % (max gene expression)	5

Electroporation in digital microfluidics	Plasmid DNA	E. Coli	1.5 ± 0.3 (cell survival)	8.6 ± 1.0 × 10^8 cfu·μg^{-1}	[6]
Vortex shedding	GFP-siRNA	HEK293 MDA-MB-231 HeLa MCF7	-	233	[7]
	miRNA	MCF7 HeLa MDA-MB-231	-	1750 1800 1100	
Vortex flow	EGFP	CHO	~ 85 %	~ 32 %	[8]
	EGFP mRNA	CD3+T	77.3 ± 0.58 %	63.6 ± 3.44 %	[9]
Hydroporation	Dextran 3kDa	MDA-MB-231	~ 97 %	85 %	[10]
	Plasmid DNA	HEK293		~ 46 %	
	DNA Nanotube	MDA-MB-231		~ 32 %	
	DNA Nanosphere	MDA-MB-231		~ 47 %	
	DNA Tetrahedron	MDA-MB-231		~ 54 %	
Spiral hydroporation	Dextran	MDA-MB-231	94 % (max.)	96.5 %	[11]

Table S2. Summary of AuNPs-mediated photoporation. siRNA: small interfering ribonucleic acid; PI: propidium iodide; QDs: quantum dots; FITC: Fluorescein isothiocyanate; pGFP: plasmid green fluorescent protein; IgG: immunoglobulin G; Au-PS: gold-polystyrene.

Shape of NMs	Size (nm)	Delivery molecule	Laser wavelength (nm)	Fluence (mJ/cm^2)	Efficiency (%)	Viability (%)	References
Sphere	250	siRNA	796	80	90	93	[12]
Rod	41 ± 5 11 ± 1	PI	1064	1 mJ	-	-	[13]
Star	55 ± 7				80		
Sphere	100	PI	532	50	25	-	[14]
			1064	1000	30		
Sphere	50	siRNA	800	-	-	-	[15]
Corrugated mushroom shape (Au-PS)	300	PI, QDs, Plasmid DNA	945	35	94 (CL1-0)	100	[16]
Sphere	100	anti-rat IgG Abs	800	80-100	-	-	[17]
Sphere	60	FITC-Dextran	532	1280	53.4	-	[18]
Sphere	70	Dextran-10000, siRNA	561	2040	-	~90 %	[19]
Corrugated mushroom shape (Au-PS)	300	PI	680	45	89.6 ± 2.8	97.4 ± 0.4	[20]
Star	-	PI, pGFP	800	-	95± 5 (pGFP)	92 ± 7 (pGFP)	[21]
Rod	-	antibody	532 or 730	2000-4500	80 (532 nm)	-	[22]
Sphere	100	Plasmid DNA	800	100	70	80	[23]
Au NPs layer	-	Dextran, GFP	808	1 Wcm^{-2}	53	19	[24]

Fabrication of flow-focusing microfluidic device

Device was fabricated using soft lithography procedure. Briefly, a silicon wafer was washed using Piranha solution (hydrogen peroxide: sulfuric acid = 1:7), followed by acetone and isopropyl alcohol (IPA) washing and drying by nitrogen blow. Then, a 150 µm thick coating of photoresist (SU-8 3050) was achieved using a double spin coating procedure. Baking at 110 ^{0}C was carried out immediately after each coating, and a longer temperature treatment was performed after the second coating to adhere the SU-8 layer properly on top of the wafer. Then, exposed to UV to pattern the microchannels design on SU-8 coated wafer. Next, post-exposure baking was performed till the patterns become visible. Then, it was treated under SU-8 developer solution, followed by immediate washing with acetone and IPA, and dried by nitrogen blow for the complete pattern development. Later, PDMS was formulated by mixing the silicone elastomer base and curing agent in a 10:1 ratio (PDMS Sylgard 184 from Dow Corning) and was poured on top of the SU-8 pattern and kept at 60 ^{0}C for 4 hrs. for curing. Once PDMS cured properly, it was easily peeled-off from the SU-8 mould. Then, the final device was formed by bonding the peeled PDMS layer and glass substrate after performing oxygen plasma treatment for 1 min. Then, temperature treatment was carried out to strengthen the bonding. Tubings were connected to the inlets and outlet for further usage. The height of the microfluidic channel was confirmed by performing profilometry analysis using a surface profiler Veeco Nt-1100 Profiler.

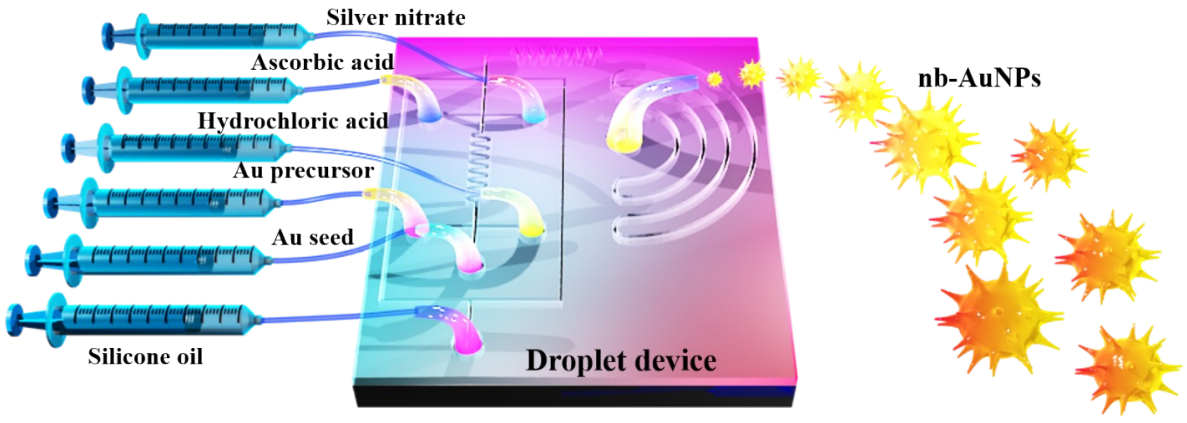

Figure S1. Schematic drawing of nb-AuNPs synthesis in microfluidic platform. Au precursor, Au seed and hydrochloric acid solutions meet in cross junction and mix well in winding geometry, later it meets with ascorbic acid and silver nitrate followed by forming reagents droplets in the last junction (flow-focusing). Winding and semi-spiral geometry provide rapid and homogenous mixing of reagents. Finally, nb-AuNPs collects in the PEG solution kept at ice-cold temperature.

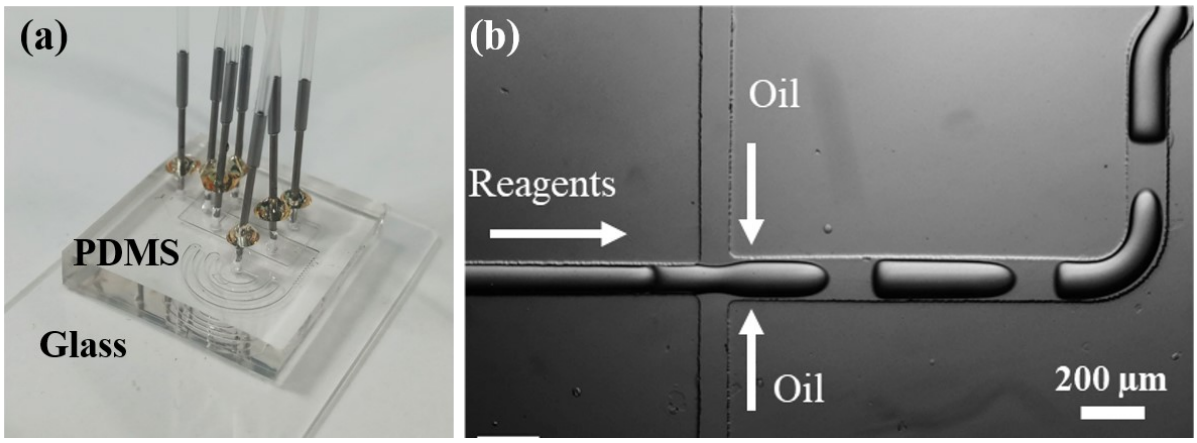

Figure S2. Microdroplets generation in the flow-focusing device. **(a)** photograph of the final fabricated device with tubes connected to the inlets and outlet. **(b)** microscopic image of microdroplet generation in the same device at a total reagent flow rate of 900 µL/h and *Q* of 6.

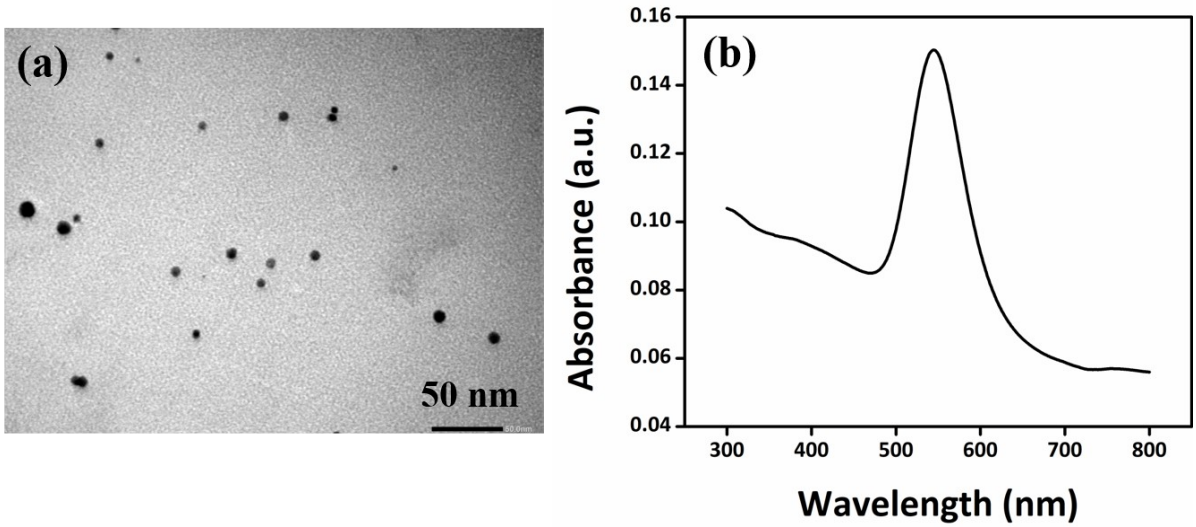

Figure S3. Characterization of citrate-stabilized Au seeds. **(a)** TEM micrograph and **(b)** UV-Vis absorption spectrum.

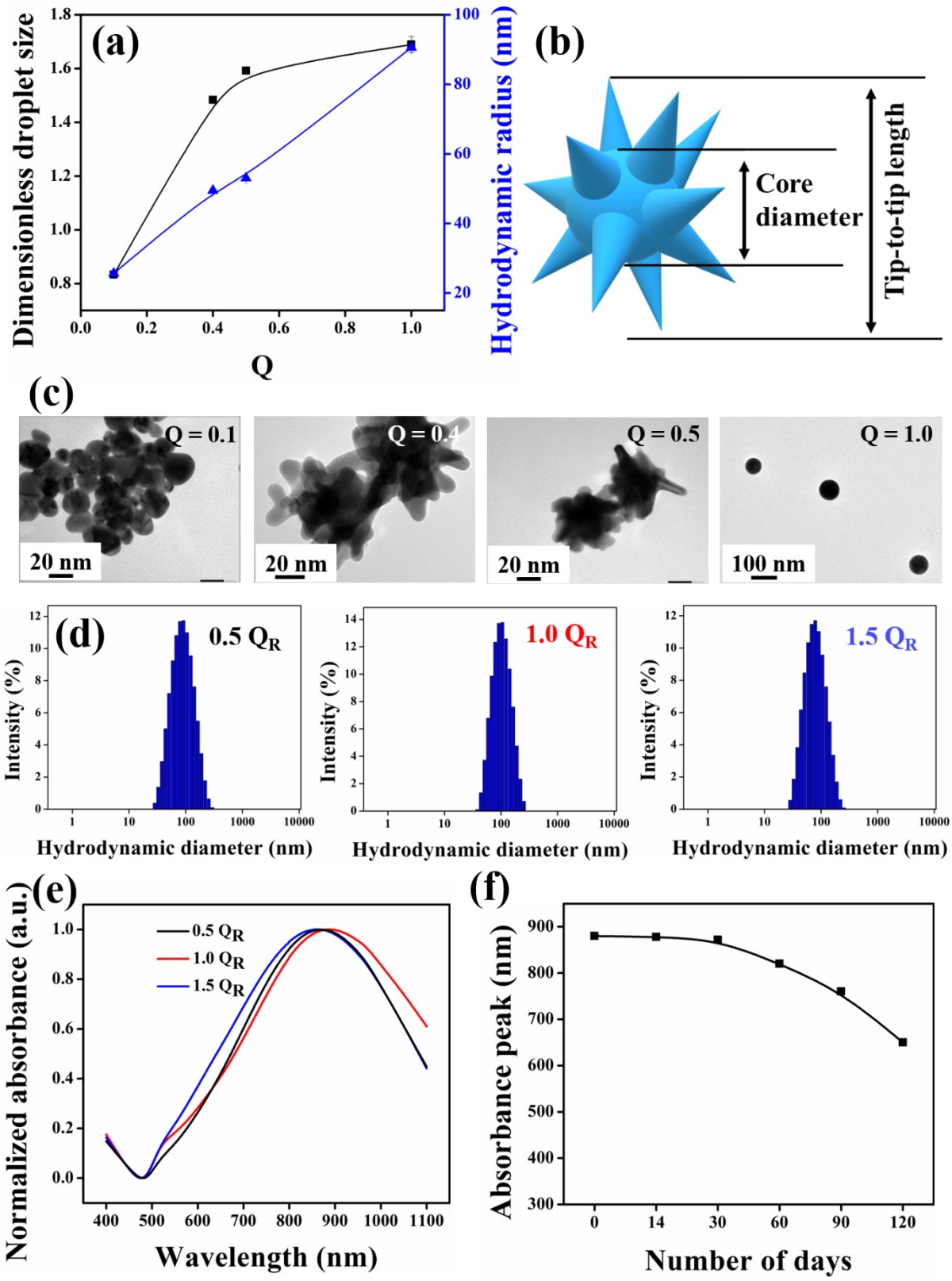

Figure S4. Optimizing the nb-AuNPs formation. **(a)** droplet size and hydrodynamic radius of NPs generated at various Q. **(b)** schematic illustration of single nb-AuNPs. 3D nb-AuNPs consists of a middle core specified by core diameter and several branches in the shape of cone attached to the core surface. Each nb-AuNPs can be represented in 2D with its core diameter, tip-to-tip length, and the number of branches. **(c)** TEM micrographs of gold nanostructures synthesized at various Q. **(d)** DLS size distribution and **(e)** UV-Vis absorbance spectra of nb-AuNPs synthesized at various seed flow rates. **(f)** UV-Vis absorbance peaks of synthesized nb-AuNPs in phosphate buffered solution (PBS) at various time duration.

Table S3. Surface zeta potential of nb-AuNPs with other morphology to evaluate the colloidal stability.

S. No	Particle shape	Max. surface zeta potential (mV)	Ref.
1	Nanostars	< -30	[25]
2	Sphere	44	[26]
3	Short nanorod	~ 42.5	[26]
4	nb-AuNPs	-45	Present work

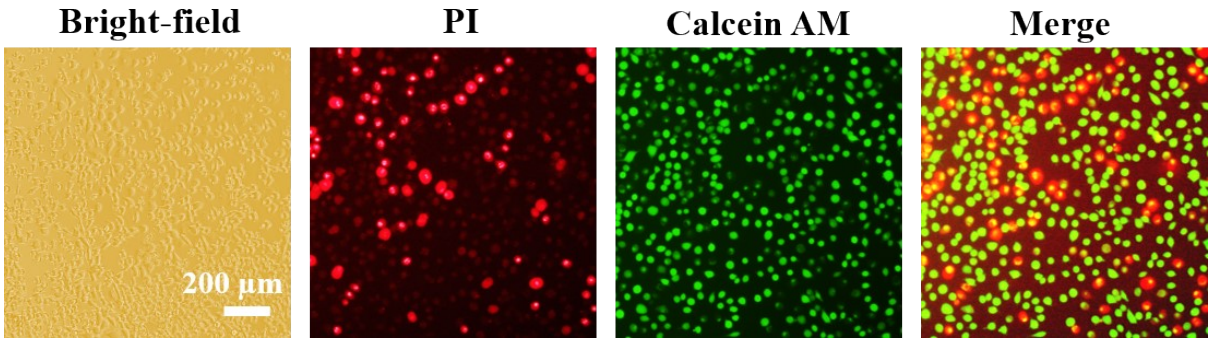

Figure S5. PI delivery using nb-AuNPs-sensitized photoporation in SiHa cells at beyond 60 s exposure time. Bright-field, fluorescence and merge images after PI delivery experiments using laser energy of 6.5 mJ (872 nm) and exposure time of 65 s.

Table S4. Quantification PI delivery results using nb-AuNPs synthesized at various flow rate of $AgNO_3$ and other reagents at 180 µL/h. Concentration of $AgNO_3$ was kept at 0.3 mM.

Flow rate (µL/h)	Laser wavelength (nm)	Efficiency (%)	Viability (%)
Q_R	720	97.34	99.26
$2Q_R$	872	99.00	99.85
$3Q_R$	910	95.23	99.00

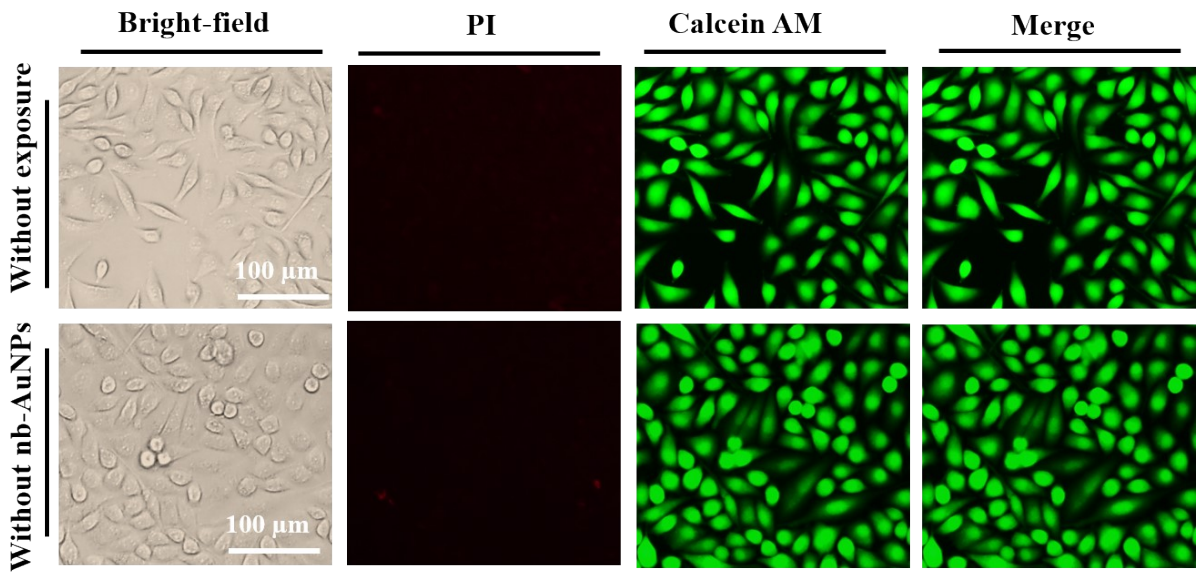

Figure S6. PI delivery using nb-AuNPs stimulated photoporation in controls. Without laser exposure (1st row) and without adding nb-AuNPs (2nd row) does not deliver PI dye into the SiHa cells. Green fluorescence shows that cells are viable and exposure was carried out at 872 nm for 15 s.

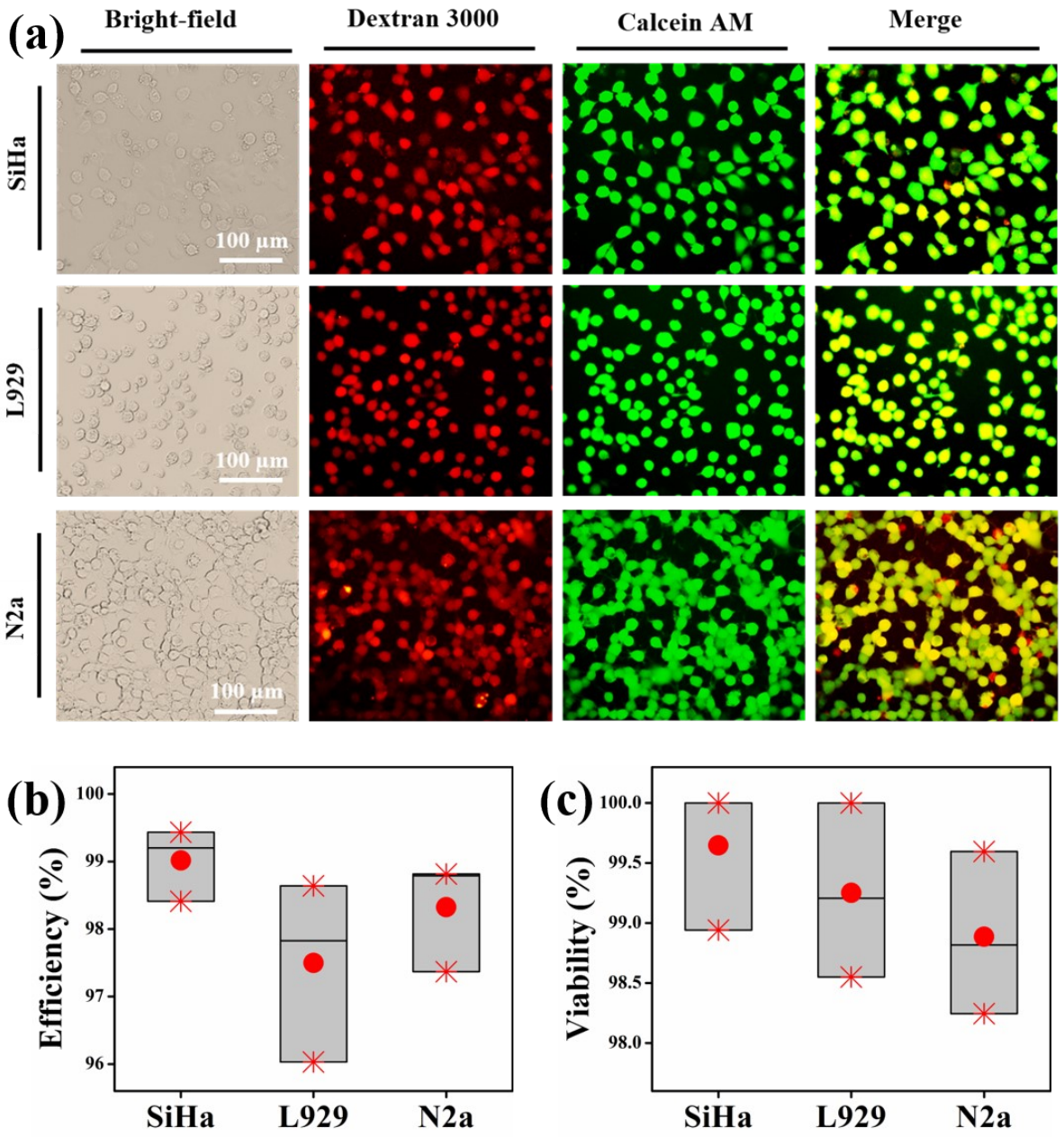

Figure S7. Dextran 3000 Da molecular delivery into mammalian cells using nb-AuNPs stimulated photoporation. **(a)** successful delivery of dextran 3000 into SiHa, L929 and N2a cells revealed by the red fluorescence signal and viability was accessed by the Calcein AM (green). Photoporation was performed at 872 nm (6.5 mJ energy) for 15 s. **(b)** quantification of cell viability after Dextran 3000 molecular delivery into SiHa, L929 and N2a. All the cell line possesses more than 98 % cell viability. **(c)** efficiency is higher in SiHa, followed by N2a, then L929 (n=3 independent experiments, data are presented as a minimum, mean, median and maximum value).

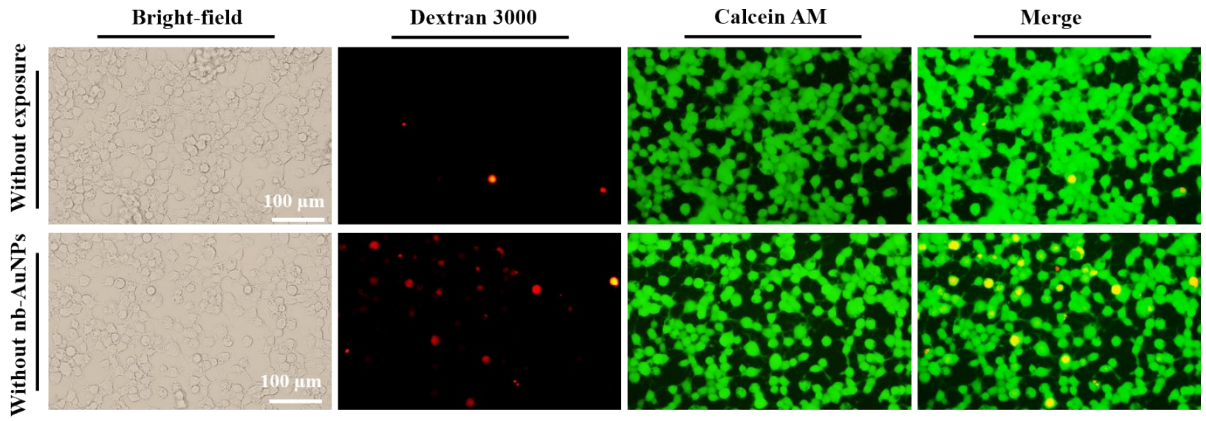

Figure S8. Dextran 3000 delivery using nb-AuNPs stimulated photoporation in controls. Without laser exposure, there is no red signal, hence no delivery. However, in laser exposure without adding nb-AuNPs, nearly 1 % cells delivered due to endocytosis. Green fluorescence shows that cells are viable and exposure was carried out at 872 nm (6.5 mJ) for 15 s.

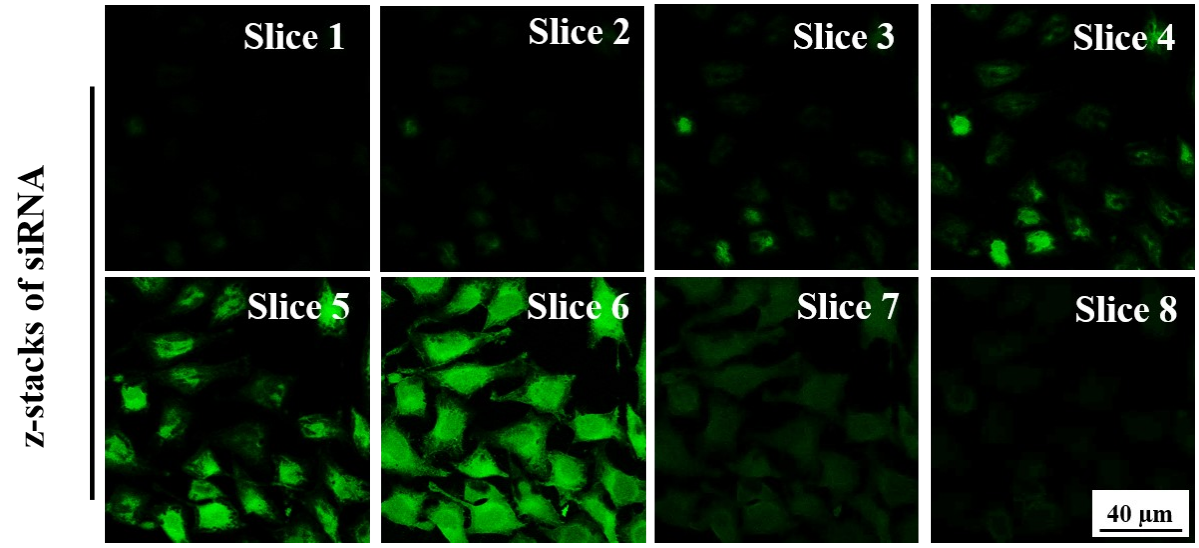

Figure S9. Slices of horizontal planes of L929 cells 24 hr after nb-AuNPs-sensitised photoporation for siRNA delivery. Spacing between successive slices is 2 µm.

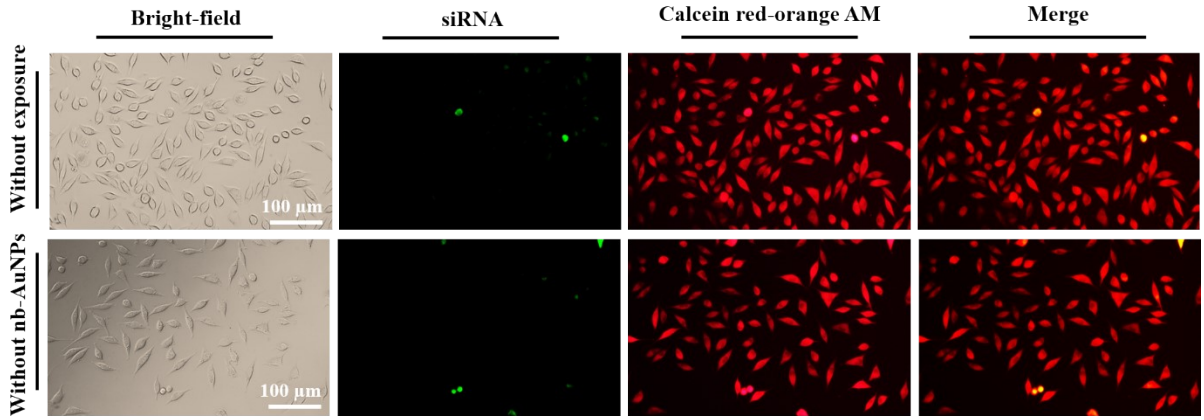

Figure S10. siRNA delivery using nb-AuNPs-mediated photoporation in controls. Without laser exposure (1st row) and without adding nb-AuNPs (2nd row), there is no delivery in L929 cells. Green fluorescence shows that cells are viable and exposure was carried out at 872 nm (6.5 mJ) for 15 s.

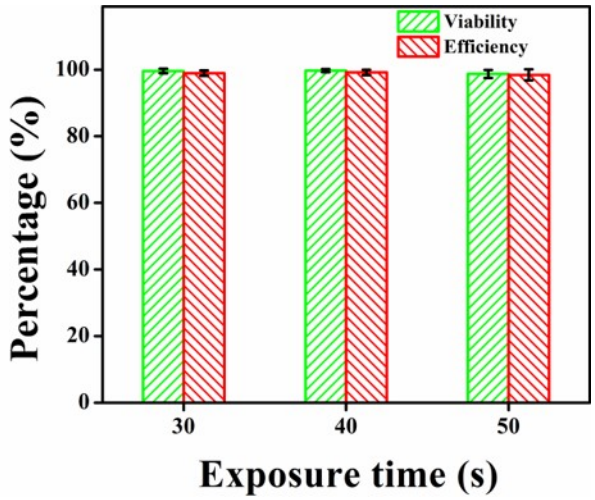

Figure S11. Plasmid delivery via nb-AuNPs mediated photoporation. Delivery efficiency and cell viability of EGFP expression plasmid delivery in SiHa cells under laser exposure of 6.5 mJ at 872 nm for various time duration (n=3 independent experiments, data are presented as mean ± s.d.).

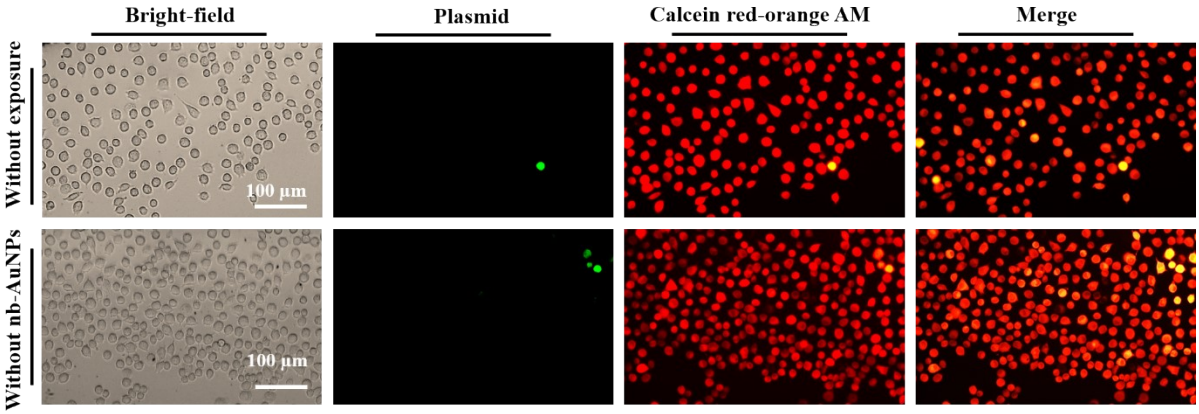

Figure S12. Plasmid delivery using nb-AuNPs stimulated photoporation in controls. Without laser exposure (1st row) and without adding nb-AuNPs (2nd row), plasmid is not delivered into SiHa cells. Green fluorescence shows that cells are viable and exposure was carried out at 872 nm (6.5 mJ) for 30 s.

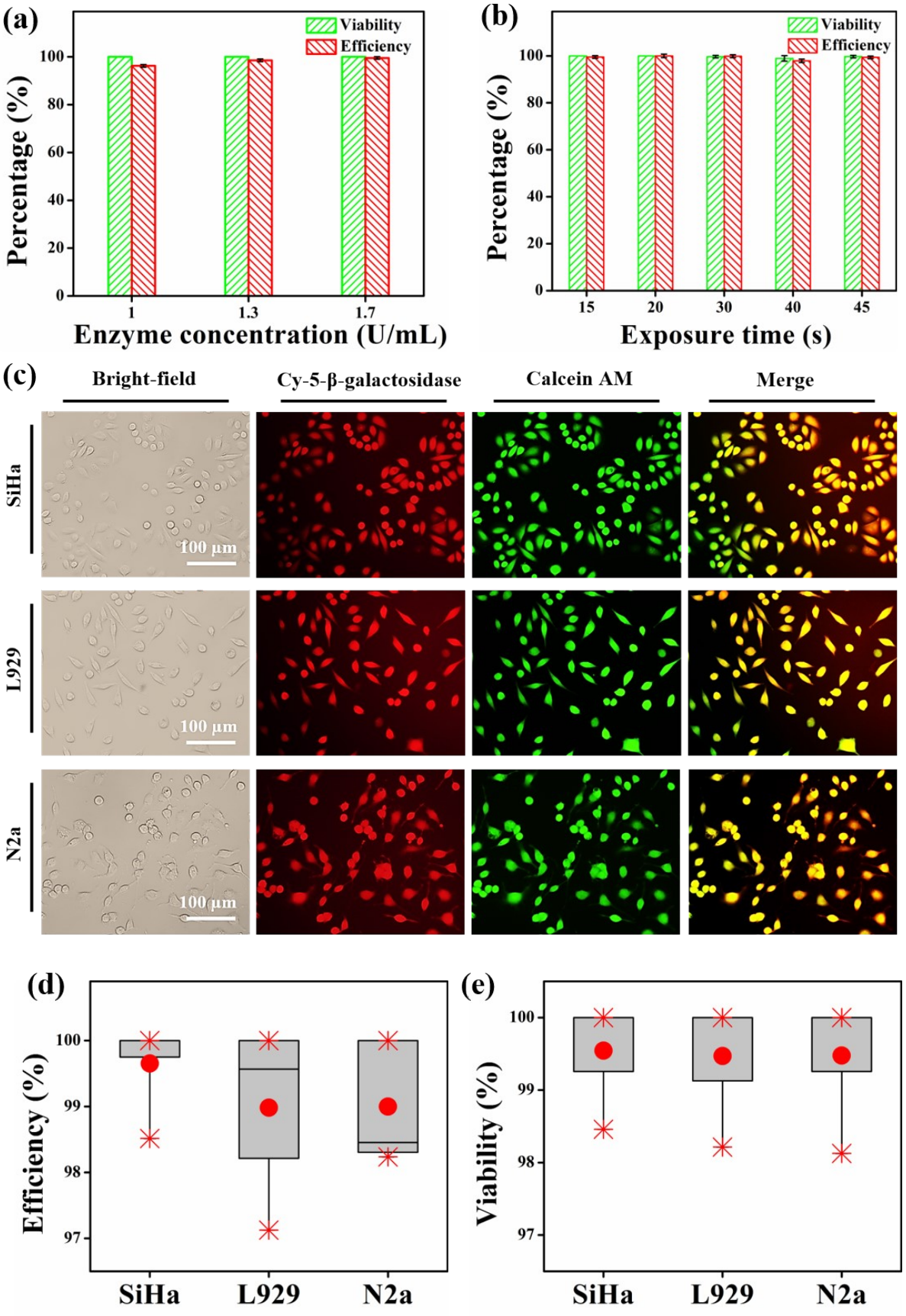

Figure S13. Cy-5-β-galactosidase enzyme delivery into mammalian cells using nb-AuNPs mediated photoporation. (**a**) Analysis of delivery efficiency and cell viability of enzyme delivery into SiHa cells under various concentration of enzyme for 15 s of laser exposure (n=3 independent experiments, data are presented as

mean ± s.d.). (**b**) Time dependent laser exposure for enzyme delivery into SiHa cells at 1.7 U/mL of enzyme concentration. (**c**) fluorescence images of enzyme delivery into SiHa, L929 and N2a cells using 1.7 U/mL of enzyme at a laser exposure of 6.5 mJ at 872 nm for 20 s. red and green fluorescence show the successful delivery of enzyme and live cells, respectively. **(d)** delivery efficiency and **(e)** cell viability comparison in all the cell lines (n=5 independent experiments, data are represented as average, minimum and maximum value).

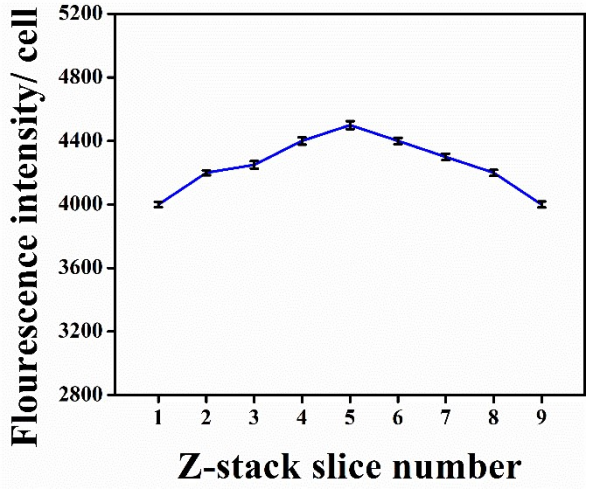

Figure S14. Quantification of fluorescence intensity/ cell from the merged images of confocal images after performing nb-AuNPs mediated photoporation (872 nm, 6.5 mJ, 45 s) for enzyme delivery in SiHa cells (n=3 independent experiments, data are presented as mean ± s.d.).

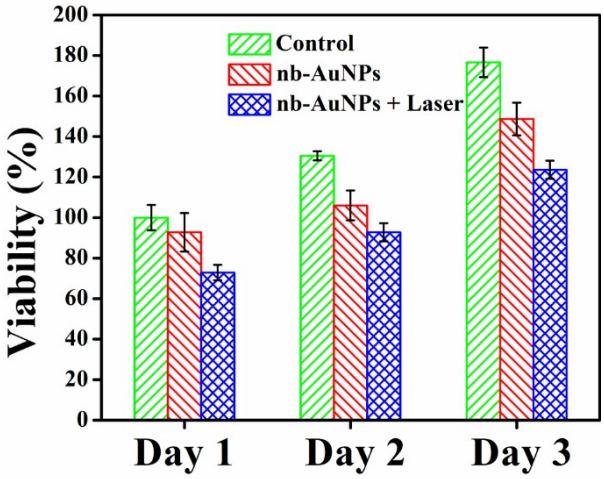

Figure S15. Toxicity analysis of nb-AuNPs-mediated photoporation. MTT Assay result shows that there is significant increase in cell viability in control, nb-AuNPs treated and nb-AuNPs + Laser treated SiHa cells (n=3 independent experiments, data are presented as mean ± s.d.).

Table S5. Quantification of intracellular delivery results using nb-AuNPs sensitized photoporation and other shapes of AuNPs in delivering PI dye.

Shape	Average size (nm)	Exposure time (s)	Laser energy (mJ)	Efficiency (%)	Viability (%)
Sphere	50	30	7.00	85.35	95.23
Dumbbell-shaped rod	60	20	6.85	92.16	89.20
Star	65	15	6.50	99.00	99.85

Table S6. Comparison of reported branched AuNPs-mediated photoporation for intracellular delivery with our intracellular delivery platform.

Size (nm)	**Plasmonic enhancement**	**Delivery molecules**	**Cells**	**Laser wavelength (nm)**	**Fluence (mJ/cm^2)**	**Efficiency (%)**	**Viability (%)**	**Ref.**
60	-	siRNA, mRNA, Cas-9 ribonucleoprotein	Human retinal pigment epithelial cells	750 ± 25	0.38	95 (max.)	92 (max.)	[27]
55 ± 7	-	PI	HeLa	1064	1 mJ	80	-	[13]
70 ± 18	-	PI, pGFP	HeLa	800	-	95± 5 (pGFP)	92 ± 7 (pGFP)	[21]
65 ± 3	200	PI, Dextran, siRNA, DNA plasmid, Enzyme, Cas-9 plasmid	SiHa L929 N2a	872	5.75	99 (max.)	100 (max.)	Present work

Table S7. Comparison of delivery efficiency of our platform with benchtop electroporator for the same biomolecule.

Molecule	Cell	Electroporator type	Delivery efficiency	Our work	Fluorescent intensity	Ref.
siRNA	HEK293	Microscale Symmetrical Electroporator	~ 31 %	~ 99 % in SiHa (our work)	233	*Sci. Rep.*, 7(2017), 1–11
Protein (66 kDa)	HEK293	Microscale Symmetrical Electroporator	71 %	~ 100 % in SiHa (our work), enzyme (465 kDa)	-	*Sci. Rep.*, 7(2017), 1–11
GFP plasmid	CT26 K562	Microfluidic-nanosecond pulse electroporation	< 60 % ~ 65 %	~ 99.2 % in SiHa (our work)	-	*Sci. Rep.*, 10(2020), 6061

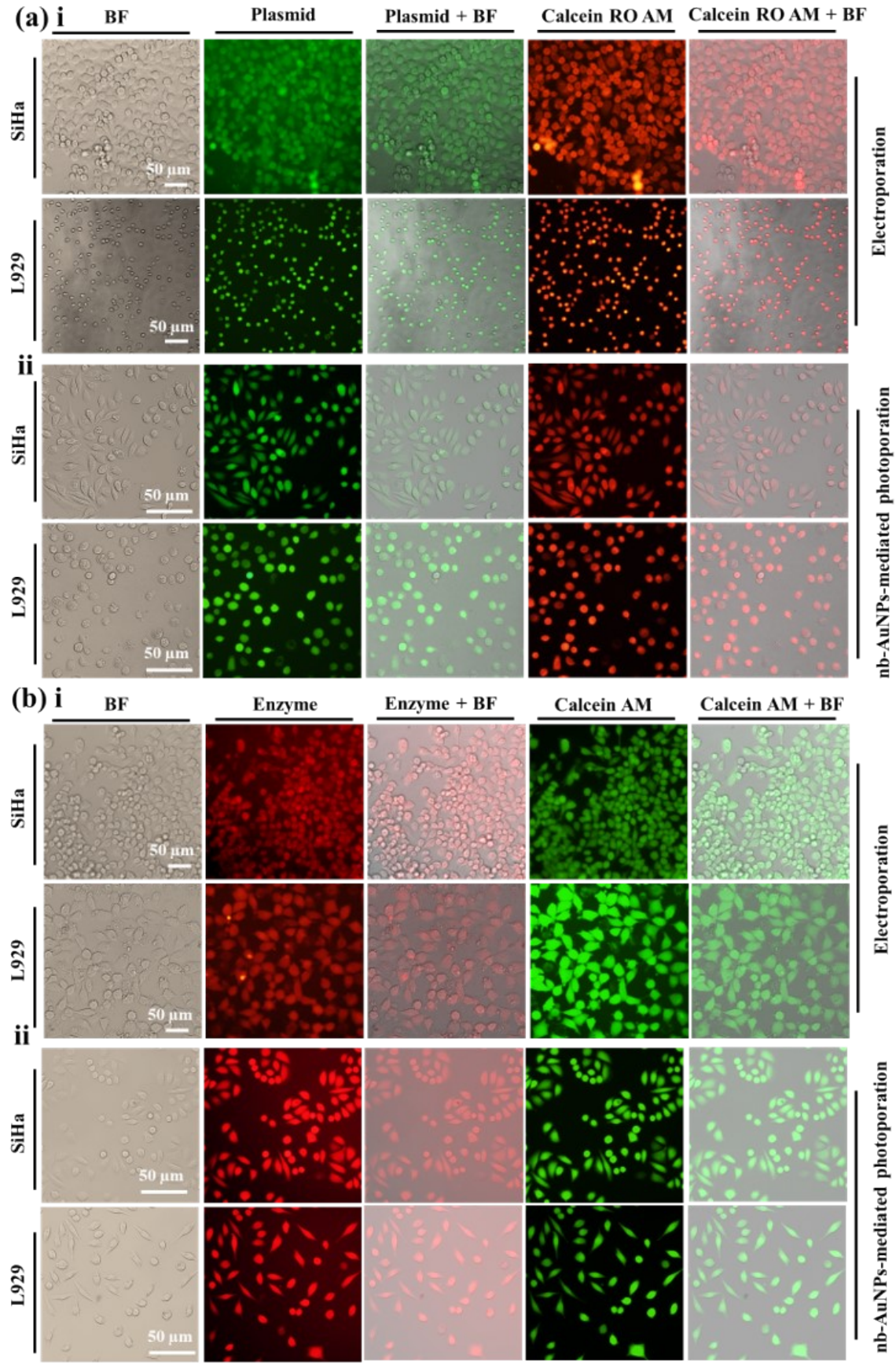

Figure S16. Representative microscopic images captured after electroporation. **(a)** plasmid and **(b)** enzyme delivery. BF (bright-field); Calcein RO (Calcein red-orange).

Cost distribution of nb-Au NPs-mediated photoporation

The details of cost calculation of individual items/parts of nb-AuNPs-mediated photoporation are described as follows.

The cost of laser equipment is 33,000 USD, and has a lifetime of ~ 10,000 hrs. On average, a single photoporation experiment long for ~ 30 sec. Hence, for 1 experiment, the laser cost is 0.0275 USD.

For device fabrication, SU-8 cost is 500 USD for 1 L, which can fabricate ~ 2500 devices (a single wafer with 10 devices requires ~ 4 mL of SU-8). On average, for single device, SU-8 cost is 0.2 USD. Silicon wafer cost is 29.5 USD per pieces, which constitute 10 devices mould, and single wafer mould can be used for 10-20 experiments. Hence, for single device, wafer cost is 0.1475 USD. Likewise, PDMS cost is 162 USD per kg. For single wafer (10 devices), we use ~ 7.6 mg of PDMS. Additionally, each device is reusable (10 times) for synthesis. Therefore, for single device, the PDMS cost is 0.0012 USD. In total, the device cost is 0.3487 USD (0.2+0.1475+0.0012). Total two devices were employed for synthesizing nb-Au NPs needed for all delivery experiments. Hence, device cost for total photoporation experiment is 0.6974 USD, and the average cost is ~ 0.006974 USD.

For synthesis, all the chemicals cost ~ 200 USD (original reagents cost), that can synthesize particles ~ 80 or more experiments due to low reagent consumption. The cost reduces to 2.5 USD, and due to reusability (10 experiments in single device) of the device, the overall cost reduces to 0.25 USD.

Biological cost comes ~ 1000 USD, which includes cost of cell culture media, essentials, biomolecules, and purchased cells. For single photoporation experiment, average cost comes ~ 0.5 USD.

The total cost of photoporation experiment is 0.78 USD (0.0275+0.06974+0.25+0.5).

Table S8. Cost distribution of nb-Au NPs-mediated photoporation experiment

Parts of the proposed delivery tool	**Cost for single photoporation experiment (in USD)**
1. Laser	0.0275
2. Device	0.006974
3. Synthesis	0.25
4. Biological items	0.5
Total	**0.78**

REFERENCES

1 A. Sharei, J. Zoldan, A. Adamo, W. Y. Sim, N. Cho, E. Jackson, S. Mao, S. Schneider, M.-J. Han, A. Lytton-Jean, P. A. Basto, S. Jhunjhunwala, J. Lee, D. A. Heller, J. W. Kang, G. C. Hartoularos, K.-S. Kim, D. G. Anderson, R. Langer and K. F. Jensen, *Proc. Natl. Acad. Sci.*, 2013, **110**, 2082–2087.

2 J. N. Belling, L. K. Heidenreich, J. H. Park, L. M. Kawakami, J. Takahashi, I. M. Frost, Y. Gong, T. D. Young, J. A. Jackman, S. J. Jonas, N.-J. Cho and P. S. Weiss, *ACS Appl. Mater. Interfaces*, 2020, **12**, 45744–45752.

3 A. Liu, M. Islam, N. Stone, V. Varadarajan, J. Jeong, S. Bowie, P. Qiu, E. K. Waller, A. Alexeev and T. Sulchek, 2018, **21**, 12–17.

4 A.-Y. Chang, X. Liu, H. Tian, L. Hua, Z. Yang and S. Wang, *Sci. Rep.*, 2020, **10**, 6061.

5 X. Ding, M. P. Stewart, A. Sharei, J. C. Weaver, R. S. Langer and K. F. Jensen, *Nat. Biomed. Eng.*, 2017, **1**, 1–7.

6 A. C. Madison, M. W. Royal, F. Vigneault, L. Chen, P. B. Griffin, M. Horowitz, G. M. Church and R. B. Fair, *ACS Synth. Biol.*, 2017, **6**, 1701–1709.

7 M. Ouyang, W. Hill, J. H. Lee and S. C. Hur, *Sci. Rep.*, 2017, **7**, 1–11.

8 J. Wang, Y. Zhan, V. M. Ugaz and C. Lu, *Lab Chip*, 2010, **10**, 2057–2061.

9 J. A. Jarrell, A. A. Twite, K. H. W. J. Lau, M. N. Kashani, A. A. Lievano, J. Acevedo, C. Priest, J. Nieva, D. Gottlieb and R. S. Pawell, *Sci. Rep.*, 2019, **9**, 3214.

10 Y. Deng, M. Kizer, M. Rada, J. Sage, X. Wang, D. Cheon and A. J. Chung, *Nano Lett.*, 2018, **18**, 2705–2710.

11 G. Kang, D. W. Carlson, T. H. Kang, S. Lee, S. J. Haward, I. Choi, A. Q. Shen and A. J. Chung, *ACS Nano*, 2020, **14**, 3048–3058.

12 M. Schomaker, D. Heinemann, S. Kalies, S. Willenbrock, S. Wagner, I. Nolte, T. Ripken, H. M. Escobar, H. Meyer and A. Heisterkamp, *J. Nanobiotechnology*, 2015, **13**, 10.

13 O. Bibikova, P. Singh, A. Popov, G. Akchurin, A. Skaptsov, I. Skovorodkin, V. Khanadeev, D. Mikhalevich, M. Kinnunen, G. Akchurin, V. Bogatyrev, N. Khlebtsov, S. J. Vainio, I. Meglinski and V. Tuchin, *Laser Phys. Lett.*, 2017, **14**, 055901.

14 B. S.-L. Lalonde, É. Boulais, J.-J. Lebrun and M. Meunier, *Biomed. Opt. Express*, 2013, **4**, 490.

15 A. M. Wilson, J. Mazzaferri, É. Bergeron, S. Patskovsky, P. Marcoux-Valiquette, S. Costantino, P. Sapieha and M. Meunier, *Nano Lett.*, 2018, **18**, 6981–6988.

16 T. S. Santra, S. Kar, T.-C. Chen, C.-W. Chen, J. Borana, M.-C. Lee and F.-G. Tseng, *Nanoscale*, 2020, **12**, 12057–12067.

17 E. Bergeron, C. Boutopoulos, R. Martel, A. Torres, C. Rodriguez, J. Niskanen, J. J. Lebrun, F. M. Winnik, P. Sapieha and M. Meunier, *Nanoscale*, 2015, **7**, 17836–17847.

18 X. Du, J. Wang, L. Chen, Z. Zhang and C. Yao, *Membranes (Basel).*, 2021, **11**, 550.

19 R. Xiong, K. Raemdonck, K. Peynshaert, I. Lentacker, I. De Cock, J. Demeester, S. C. De Smedt, A. G. Skirtach and K. Braeckmans, *ACS Nano*, 2014, **8**, 6288–6296.

20 P. Gupta, S. Kar, A. Kumar, F.-G. Tseng, S. Pradhan, P. Sinha Mahapatra, T. Subhra Santra, P. S. Mahapatra and T. S. Santra, *Analyst*, 2021, **146**, 4756–4766.

21 T. Pylaev, E. Vanzha, E. Avdeeva, B. Khlebtsov and N. Khlebtsov, *J. Biophotonics*, 2019, **12**, e201800166.

22 C. Yao, F. Rudnitzki, Y. He, Z. Zhang, G. Hüttmann and R. Rahmanzadeh, *J. Biophotonics*, 2020, **13**, e202000017.

23 J. Baumgart, L. Humbert, É. Boulais, R. Lachaine, J. J. Lebrun and M. Meunier, *Biomaterials*, 2012, **33**, 2345–2350.

24 Z. Lyu, F. Zhou, Q. Liu, H. Xue, Q. Yu and H. Chen, *Adv. Funct. Mater.*, 2016, **26**, 5787–5795.

25 M. K. Hameed, J. B. M. Parambath, M. T. Gul, A. A. Khan, Y. Park, C. Han and A. A. Mohamed, *Appl. Surf. Sci.*, 2022, **583**, 152504.

26 S. Park, N. Sinha and K. Hamad-Schifferli, *Langmuir*, 2010, **26**, 13071–13075.

27 M. H. Kafshgari, L. Agiotis, I. Largillière, S. Patskovsky and M. Meunier, *Small*, 2021, **17**, 2007577.